ACS APPLIED ENERGY MATERIALS

www.acsaem.org Article

Phosphorus-Functionalized Organic Linkers Promote Polysulfide Retention in MOF-Based Li−S Batteries

Avery E. Baumann, Rasha I. Anayah, and V. Sara Thoi*

Cite This: https://doi.org/10.1021/acsaem.2c02925 Read Online

ACCESS | Metrics & More | Article Recommendations | Supporting Information

ABSTRACT: Metal−organic frameworks (MOFs) have been an area of intense research for their high porosity and synthetic tunability, which afford them controllable physical and chemical properties for various applications. In this study, we demonstrate that functionalized MOFs can be used to mitigate the so-called polysulfide shuttle effect in lithium−sulfur batteries, a promising next-generation energy storage device. UiO-66-OH, a zirconium-based MOF with 2-hydroxyterephthalic acid, was functionalized with a phosphorus chloride species that was subsequently used to tether polysulfides. In addition, a molecular chlorophosphorane was synthesized as a model system to elucidate the chemical reactivity of the phosphorus moiety. The functionalized MOFs were then used as a cathode additive in coin cell batteries to inhibit the dissolution of polysulfides in solution. Through this work, we show that the functionalization of MOF with phosphorus enhances polysulfide redox and thereby capacity retention in Li−S batteries. While demonstrated here for polysulfide tethering in batteries, we envision this linker functionalization strategy could be more broadly utilized in separations, sensing, or catalysis applications.

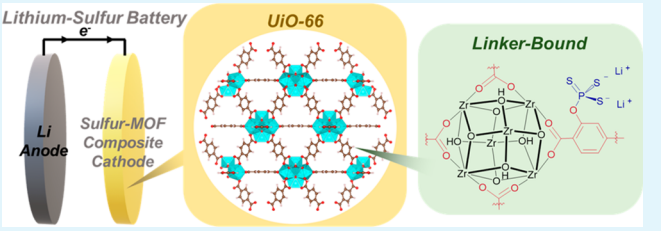

KEYWORDS: *metal−organic framework, post-synthetic modification, electrochemical cells, polysulfide, linker functionalization, thiophosphate*

INTRODUCTION

Lithium−sulfur (Li−S) battery technology is emerging as a key contender for next-generation energy storage devices. However, the mechanism of energy storage in conventional Li−S batteries relies on conversion reactions segmenting elemental sulfur (S_8) to intermediate-length polysulfides (Li_2S_n, n = 4−8), down to insoluble Li_2S/Li_2S_2. In this process, the generated polysulfides can diffuse away from the electrode and limit cell capacity via the loss of active material and deleterious deposition elsewhere in the cell. The leaching of active material contributes to a continuous loss in capacity as the cell cycles. One strategy to combat the leaching phenomenon is to chemically tether sulfur species to the cathode architecture, thereby maintaining device capacities over longer operational lifetimes.

Thiophosphate additives are known to influence electrochemical performance in Li−S systems by coordinating with polysulfides, decreasing polysulfide leaching, and lowering redox polarization during charge/discharge.[1−10] In our previous work, we incorporated lithium thiophosphate into Zr MOFs via a chemical reaction with the coordinatively unsaturated metal node.[3] The extent of thiophosphate incorporation was controllable by adjusting both the quantity of open binding sites on the Zr node and the stoichiometric equivalents of Li_3PS_4 used in the synthesis. Ultimately, we found the thiophosphate-functionalized MOFs improved sulfur utilization and capacity retention when implemented in Li−S battery cathodes either in physically mixed MOF−sulfur composites or where sulfur had been infiltrated into the MOF.[3,6]

Using this node-bound strategy as inspiration, we sought to develop a new method to increase the phosphorus content incorporated in the MOF structure and expand the range of MOFs that could be utilized by functionalizing the organic linker. In UiO-66, the chemical structure of the MOF contains six ditopic benzene dicarboxylate (BDC) linkers per formula unit $(Zr_6(\mu_3\text{-}OH)_4(\mu_3\text{-}O)_4(BDC)_6)$.[11] Even in the most defected UiO-66 samples, the maximum number of open sites capable of binding phosphates is roughly three per formula unit.[12,13] Therefore, utilization of the linker sites represents an alternative strategy to increase the concentration of phosphosulfides in the functionalized MOF. This strategy is notably different from our previous node functionalization method as it relies on the irreversible organic transformation of the linker, rather than coordination at the metal node, to secure the phosphorus moiety.

Received: September 9, 2022
Accepted: November 10, 2022

We targeted post-synthetic functionalization strategies, rather than synthesizing the MOF with a thiophosphate linker or linker-exchange, because of the known binding capabilities of the metal node with phosphorus species and the chemical sensitivity of P−S compounds.[3,14−17] Herein, we present a synthetic route to incorporate PCl_5 with labile P−Cl bonds into UiO-66-OH, a derivative of UiO-66. The strength of the P−O bond secures the phosphorus atom to the linker, while the remaining P−Cl bonds are exchangeable with sulfide ligands to create a covalently tethered thiophosphate molecule. We offer spectroscopic evidence to confirm these synthetic manipulations, including parallel demonstrations of analogous chemistry in a molecular model system, and investigate the role of organophosphorus additives in Li−S electrochemistry.

RESULTS AND DISCUSSION

PCl_5 is a well-known chlorinating reagent in synthetic organic chemistry and can readily react with alcohols to form alkyl chlorides via substitutive chlorination. Chlorination of aromatic alcohols (ArOH) has not been observed using PCl_5 or PCl_3, typically instead forming substituted chlorophosphoranes $(ArO)_xPCl_{5-x}$.[18,19] We utilize analogous chemistry to install phosphorus moieties onto the MOF linker, 2-hydroxyterephthalate (BDC-OH), in UiO-66-OH to generate UiO-66-OP as illustrated in Scheme 1. Solution-state ^1H NMR

Scheme 1. Post-synthetic Functionalization of UiO-66-OH and Parallel Synthesis of Molecular AnalogMOF (Black) and Molecular (Blue) Routes of Ligand Tethering via PCl_5 and Conversion to Phosphosulfide Compounds

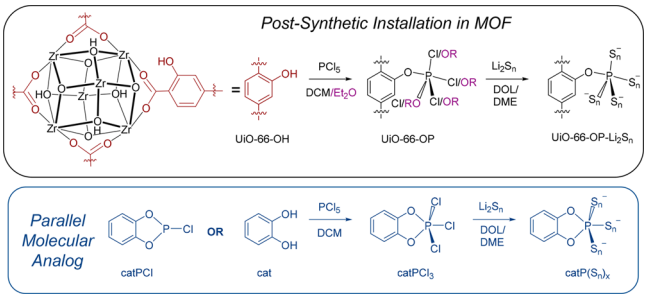

spectra were collected on MOFs digested in 1 M $NaOH/D_2O$ before and after reaction with PCl_5 (Figure 1). The digested UiO-66-OH sample yields the three expected doublets for each of the aromatic protons of BDC-OH at shifts between 6.7 and 7.1 ppm along with a singlet for formate at 8.3 ppm (Figure 1a, black). After reaction with PCl_5, the ^1H NMR spectrum of the digested UiO-66-OP sample exhibits a prominent new trio of doublets with downfield chemical shifts between 7.2 and 7.8 ppm that originate from the phosphorylated linker, BDC-OP (Figure 1b). The extra degree of splitting arises from coupling to the phosphorus nucleus bound to the linker. Some minor peaks are also observed in this region that display the characteristic trio of doublets, indicating possible trace quantities of other BDC-OP derivatives (Figure S1). A control reaction using the sodium salt of the linker BDC-OH confirms our ^1H NMR assignments for BDC-OP (Figure 1a, green).

The level of PCl_5 incorporation into UiO-66-OH can be tuned by varying the stoichiometric addition of PCl_5. We focus our discussion on two functionalized MOFs, UiO-66-OP25 and UiO-66-OP50, which are roughly 25% and 50% substituted, respectively (Figure S1, Table S1). The ^{31}P NMR spectra obtained from the same set of samples (Figure S2) exhibit peaks for hydrolyzed PCl_5 as PO_4^{3-} at 5.6 ppm and the hydrolyzed BDC-OP compound at 0.2 ppm, a shift in agreement with a monosubstituted phosphoester compound $(ROPO_3^{2-})$.[20] Hydrolysis of the labile P−Cl groups occurs in the presence of water, which is required for the sample digestion protocol. The peak corresponding to inorganic phosphate (5.6 ppm) persists even after repeated washing with diethyl ether (Et_2O), hinting there may also be coordination of PCl_5 to the Zr node in addition to the linker-bound species.

To further investigate this reactivity, we prepared and isolated a molecular analog, $catPCl_3$, as drawn in Scheme 1. Because of the wide range of products in the phenoxy-substituted molecular model over the catechoxy-substituted model, we focused our efforts on the latter as a model system. The model compound was obtained by reacting *o*-phenylene phosphochloridite (catPCl) and PCl_5 to form $catPCl_3$. The ^1H NMR spectrum of $catPCl_3$ shows a multiplet at 7.05 ppm (Figure S3). In addition, $catPCl_3$ is identified by a distinct ^{31}P NMR signal appearing at −26 ppm (Figure S4) as described previously.[19]

In addition to the NMR of the digested MOFs, solid state ^{31}P NMR of functionalized MOF was conducted to probe the chemical environment of the phosphorus in UiO-66-OP50 (Figure 2). The broad peak at −27 ppm in the UiO-66-OP50 sample is identical with the ^{31}P shift in $catPCl_3$ (Figure S4), indicating that the MOF has been functionalized in a manner similar to the molecular species. To assess the identity of the peak centered at −1 ppm, we subjected a high-defect UiO-66 sample, which contains open nodal Zr sites, to the PCl_5 loading procedure and found a similar shift at -1 ppm in the solid state ^{31}P NMR spectrum. In UiO-66, the linker is unfunctionalized and should not yield any incorporated organophosphorus compounds upon reaction with PCl_5. To confirm, the digested PCl_5-treated UiO-66 shows no new linker features in the solution ^1H NMR spectrum (Figure S5a,b), and the solution ^{31}P NMR spectrum exhibits only the peak at 5.6 ppm attributed to inorganic phosphate (PO_4^{3-}) (Figure S5c,d). The presence of inorganic phosphate in the solution ^{31}P NMR confirms phosphorus reactivity with the defected hexanuclear Zr cluster, which is partially bound by formate ligands. The solution ^1H NMR spectrum also shows a decrease in the formate signal relative to linker (Figure S5a,b), indicating that PCl_5 may displace the formate ligand. The peaks at −1 ppm in the solid-state ^{31}P NMR spectra (Figure 2, gray and orange) of the high-defect UiO-66 + PCl_5 and UiO-66-OP50 (i.e., UiO-66-OH + PCl_5) thus support phosphorus displacement of formate at the node. This node-bound species may be a mixture of P-bound Cl and OR (from ether used in the washing step, which can react with PCl_x species, Figure S6).

Vibrational spectroscopy is another valuable tool to investigate our functionalization methods because of the characteristic stretches of phosphorus compounds. The signals for P−O vibrations are typically very strong in Fourier-transform infrared spectroscopy (FT-IR), where different oxygen functionalities result in distinct peak positions. In Figure 3, unreacted UiO-66-OH is compared to the functionalized UiO-66-OPx solids before and after air exposure. Two peaks corresponding to the symmetric and asymmetric P−O−C stretches are observed at 1190 and 854 cm^{-1} and are denoted with an asterisk. The very strong P−OH signal is also

https://doi.org/10.1021/acsaem.2c02925
ACS Appl. Energy Mater. XXXX, XXX, XXX−XXX

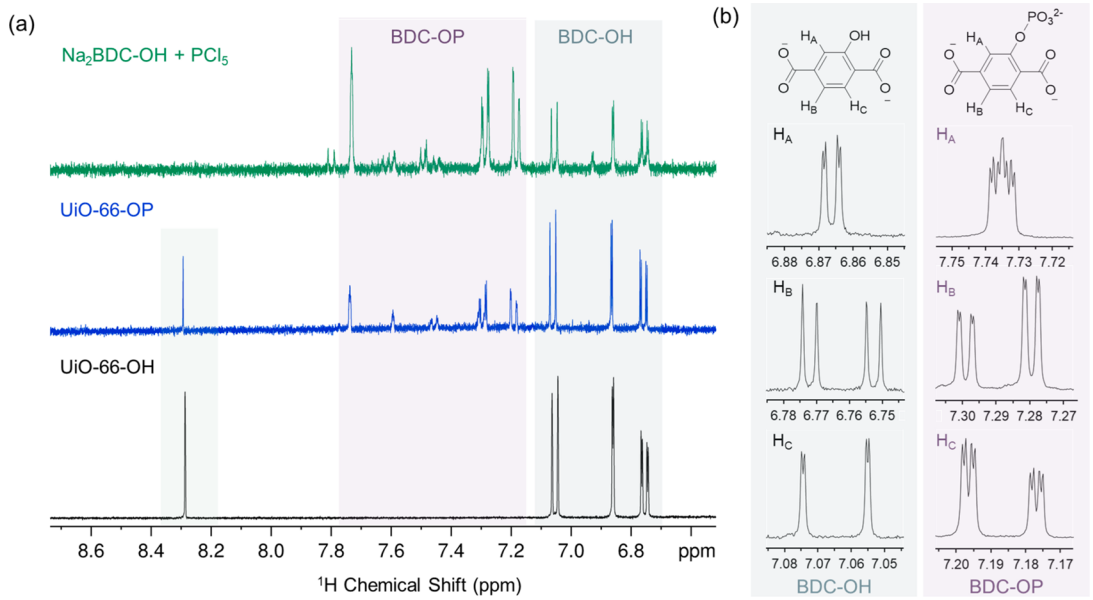

Figure 1. Solution state ^{1}H NMR spectra indicating the formation of BDC-OP species in comparison to BDC-OH. (a) The bottom two spectra were obtained from digesting UiO-66-OH and UiO-66-OP samples and contain a peak at 8.3 ppm corresponding to formate. The spectrum obtained from the reaction of Na_2BDC-OH and PCl_5 features peaks attributed to BDC-OH and BDC-OP species. All spectra were taken in 1 M NaOH in D_2O required by the MOF digestion protocol. The peak assignments and figures in (b) highlight the extra peak splitting occurring from the proximity of the aromatic protons to the phosphorus nucleus in digested UiO-66-OH (with BDC-OH linkers) and UiO-66-OP (with BDC-OP linkers).

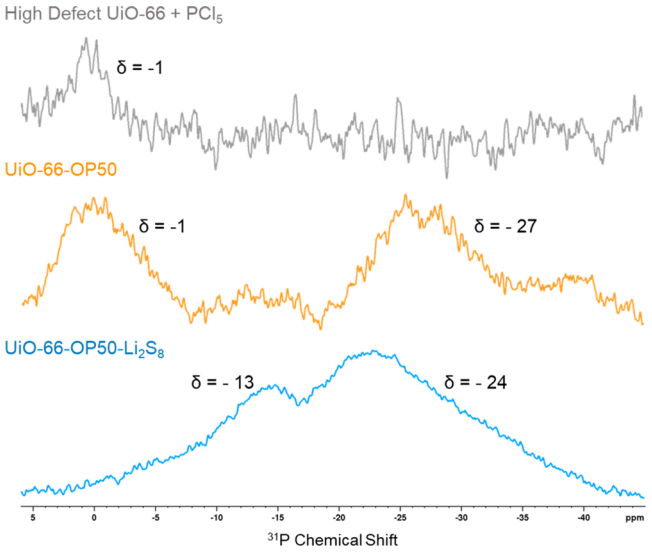

Figure 2. Solid-state ^{31}P NMR of (gray) high-defect UiO-66 + PCl_5, (orange) UiO-66-OP50, and (blue) UiO-66-OP50-Li_2S_8.

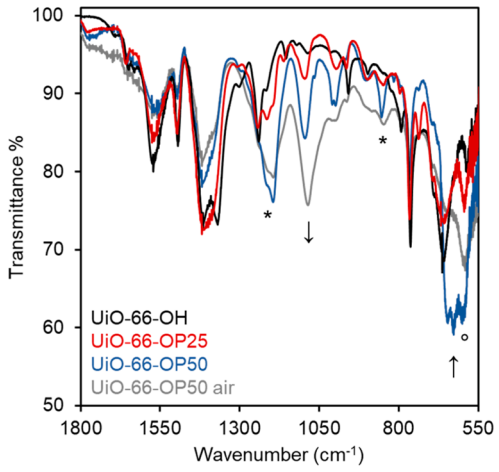

Figure 3. New features are observed for the UiO-66-OP25 and UiO-66-OP50 samples that were not present in the UiO-66-OH sample. The signals we assign to the symmetric and asymmetric P−O−C stretches (marked with ∗) persist upon air exposure. A simultaneous increase in the P−O stretch near 1100 cm^{-1} and a decrease in the P−Cl stretches near 700 cm^{-1} upon air exposure suggest P−Cl bond hydrolysis (marked with arrows). The feature around 600 cm^{-1} (marked with ○) is attributed to vibrations of the Zr node and are considerably shifted from the parent MOF feature, suggesting PCl_5 reacts with the metal node cluster as well as the organic linker.

apparent at ∼1080 cm^{-1} and grows in with continued air exposure from P−Cl bond hydrolysis. Features below 750 cm^{-1} correspond to P−Cl and nodal vibrations. The concomitant decrease in intensity of the sharp peak at 649 cm^{-1} with increase in the aforementioned P−OH stretch (at ∼1080 cm^{-1}) in the presence of air suggests the decreasing signal is related to a P−Cl vibration. We also observe broad inorganic phosphate features in FT-IR spectra of the high-defect UiO-66 + PCl_5 sample, in contrast with sharp P−O−C peaks observed in UiO-66-OPx spectra (Figure S7). Identification of inorganic phosphate in both FTIR and NMR experiments further suggests PCl_5 may react with the underlying MOF structure in high-defect UiO-66 and UiO-66-OH, albeit to a much lesser extent in UiO-66-OH.

The ratio of P to Zr by weight percent in UiO-66-OP50 was found to be 0.15 by elemental analysis (Table S2). This incorporation of P is far higher than the values obtained in our previous node functionalization approach using Li_3PS_4, which only incorporated 0.01 (wt % P/Zr) in high-defect UiO-66.[3] The loading of P can be controlled through variation of the amount of PCl_5 employed. Upon loading, the characteristic X-

https://doi.org/10.1021/acsaem.2c02925
ACS Appl. Energy Mater. XXXX, XXX, XXX−XXX

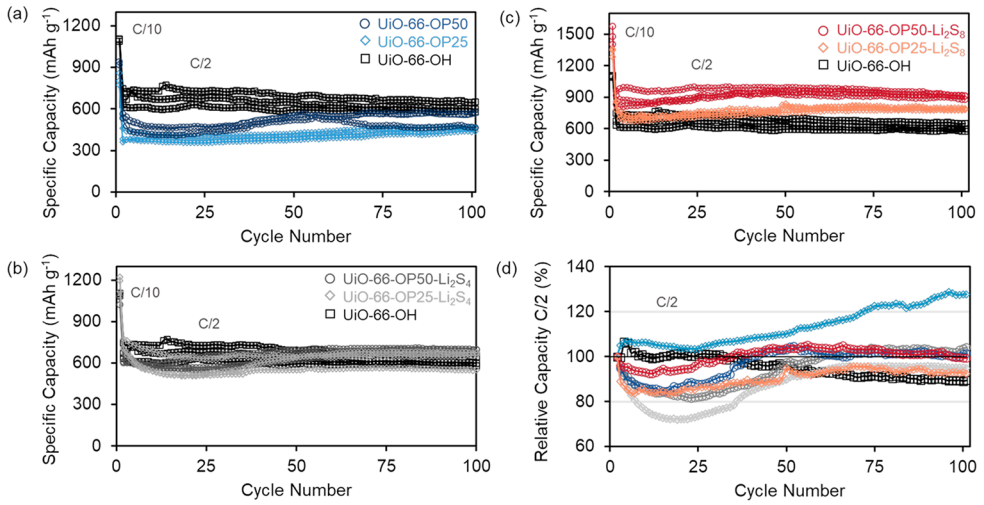

Figure 4. Galvanostatic Li−S cycling results for (a) UiO-66-OPx (washed with Et_2O, no added Li_2S_n) demonstrates the UiO-66-OP25 and UiO-66-OP50 cells deliver diminished capacity when compared to the control UiO-66-OH cells due polysulfide uptake. However, the capacity retention is excellent and appears to be increasing above 50 cycles. The samples obtained from reaction with (b) UiO-66-OPx and 10 mM Li_2S_4 and (c) UiO-66-OPx and 40 mM Li_2S_8 show similar capacity retention behavior. A portion of the capacity delivered in (b, c) arises from introduction of sulfur in the synthetic procedure. (d) Relative capacity of UiO-66-OP50 (dark blue circles), UiO-66-OP25 (light blue diamonds), UiO-66-OP50-Li_2S_8 (red circles), UiO-66-OP25-Li_2S_8 (pink diamonds), UiO-66-OP50-Li_2S_4 (dark gray circles), UiO-66-OP25-Li_2S_4 (light gray diamonds), and UiO-66-OH (black squares).

ray diffraction pattern remains unchanged from the reference UiO-66 material (Figure S8), though stoichiometric equivalency above 4 results in material degradation via our current synthesis methods. We selected UiO-66-OP25 and UiO-66-OP50 as ideal candidates to investigate phosphorus incorporation on both polysulfide capture and Li−S battery performance.

Sulfide Substitution to Yield the Thiophosphate. In the next step, we convert the labile P−Cl bonds to P−S by using solutions of lithium polysulfides (Li_2S_n, where n = 4 or 8) as shown in Scheme 1. In our molecular studies, the reaction between $catPCl_3$ and polysulfides generated a distribution of substituted products, as evidenced by ^{31}P NMR spectroscopy (Figures S3 and S4). The distribution of products is attributed to the disproportionation of lithium polysulfides in solution. Our molecular studies provided insights into P−Cl chemistry that guided the functionalization of UiO-66-OH.

After solvent exchange with Et_2O, which we have found to improve the separation of UiO-66-OPS powder, the MOF powder was soaked in the lithium polysulfide solution. Different compositions of lithium polysulfide solutions were explored to assess the ability of the phosphorus group to bind various sulfur compounds. When examining the solid-state ^{31}P NMR spectrum of the UiO-66-OP50 Li_2S_8, we observe the ^{31}P peaks shifting to slightly more positive values at −24 and −13 ppm (Figure 2, blue), both downfield from −27 ppm in UiO-66-OP50, a trend that matches our solution ^{31}P NMR studies on molecular $catPCl_3$ (Figure S4). The divergence in the absolute shifts from the molecular model is likely due to limited diffusion of long-chained polysulfides into the MOF pore. Upon exposure to air, these peaks are shifted by −10 ppm, which supports the hydrolysis of P−S bonds in air (Figure S9). It is also notable that features attributed to node-bound phosphorus at −1 ppm (Figure 2, orange) and node-bound PS_x previously observed[3] are not apparent in the UiO-66-OP50+Li_2S_8, indicating that nodal functionalization is a minor reaction in UiO-66-OP5-Li_2S_8 compared to linker functionalization.

In addition to material characterization, we provide spectroscopic evidence of polysulfide uptake using UV−vis absorbance spectroscopy, wherein aliquot volumes taken from MOF + Li_2S_8 reaction solutions were compared (Figure S10). In all cases, the solution aliquots of UiO-66-OP25 or UiO-66-OP50 with Li_2S_n exhibit lower absorbances arising from soluble polysulfide anions than the aliquots from the UiO-66-OH + Li_2S_8 control, indicating uptake into the MOF. In addition, UiO-66-OP50 removes more free polysulfide from solution than UiO-66-OP25, confirming that the phosphorus species is instrumental in promoting polysulfide uptake.

Influence of Phosphorus on Li−S Electrochemistry. The synthesized MOFs were incorporated into Li−S battery electrodes to evaluate the influence of the various phosphorus moieties on cycling chemistry. Each electrode was prepared by casting a slurry consisting of 45% S, 30% MOF, 15% carbon black (Super-P), and 10% polymer binder (PVDF) onto a preweighed carbon paper disk. After the slurry was dried, the cathode was weighed to determine the mass of sulfur and assembled into coin cells opposite a metallic Li anode. Additional detailed descriptions of the cathode preparation and coin cell construction methods are included in the Supporting Information.

We first explored the UiO-66-OPx samples, where the P−Cl groups have not been converted to P−S. Our NMR (Figure 2) and UV−vis (Figure S10) experiments demonstrate the P−Cl moiety reacts with soluble polysulfides to form P−S complexes, thus removing utilizable sulfur compounds from the electrochemically available material in the cathode. At least a portion of the sulfides cannot be recovered, as both the UiO-66-OP25 and UiO-66-OP50 cells exhibit lower capacity than the cells constructed with the parent UiO-66-OH sample (Figure 4a). Upon continued cycling, the cells containing UiO-66-OP25 and UiO-66-OP50 do not exhibit capacity decay, but rather increase in capacity over 100 cycles at C/2. The increase in capacity over cycling indicates incorporation of the phosphorus group plays a significant role in limiting polysulfide leaching and assists in accessing sulfur that may not have been utilized

https://doi.org/10.1021/acsaem.2c02925
ACS Appl. Energy Mater. XXXX, XXX, XXX−XXX

in early cycles, as suggested by previous studies.[3,10,21] The cycling experiments presented in Figure 4a provide a benchmark for our results, indicating phosphorus incorporation itself (and not addition of lithium polysulfides) is responsible for the improved capacity retention.

The next sets of battery experiments were designed to examine the functionalized MOFs containing P−S moieties. Two different polysulfide solutions (10 mM Li_2S_4 and 40 mM Li_2S_8) were used to incorporate different chain lengths of tethered polysulfide species into the MOF. Battery cycling results for the shorter chain length polysulfide samples (UiO-66-OP25-Li_2S_4 and UiO-66-OP50-Li_2S_4) in Figure 4b show both functionalized samples exhibit a small dip in capacity once the rate is shifted from C/10 to C/2 but regain performance over continued cycling. This dip and recovery indicate some polysulfides are taken up in early cycles but seem to be utilized more efficiently in later cycles. Cells containing UiO-66-OP50-Li_2S_4 recover from this dip region in fewer cycles than the UiO-66-OP25-Li_2S_4 cells, signifying the phosphorus moiety is responsible for enhancing sulfur utilization.

The cycling results from cells containing longer chain length polysulfides (UiO-66-OP25-Li_2S_8 and UiO-66-OP50-Li_2S_8) are presented in Figure 4c. These cells illustrate further improvements in sulfur utilization and capacity retention (Figure 4d) upon phosphosulfide functionalization compared to the parent UiO-66-OH cells. While some of this capacity arises from the sulfur molecules introduced from MOF synthesis, as discerned from "noS" control experiments (Table S3), the significant capacity retention over the parent MOF is again observed by the flat or increasing capacities over 100 cycles. The cells containing functionalized MOFs also retain capacity better than control sulfur/carbon (S/C) composite cathodes (Figure S11) prepared with the same sulfur loading. The combined electrochemical cycling results highlight the role of the phosphorus species in mitigating capacity fade. From these results, we hypothesize the organophosphorus species displays similar reactivity proposed for inorganic polysulfidophosphates[2] where the phosphorus atom anchors reversibly expandable polysulfide chains (Figure S11).

Because sulfur atoms are either removed or added in all of these experiments (sulfur bound directly to the phosphorus atom should not be electrochemically accessible), it is difficult to make a definitive statement regarding the effect of phosphorus on sulfur utilization. To address this, we implement a symmetric cell cyclic voltammetry experiment using electrodes containing either UiO-66-OH or UiO-66-OP25 presoaked in 40 mM Li_2S_8.[22−24] Both electrodes comprising the cell were made using a slurry of 60% carbon, 30% MOF, and 10% PVDF binder. The symmetric cell is first potentiometrically cycled in the electrolyte to establish a baseline current response (Figure 5, black curves), then opened, and reassembled (using the same electrodes and separators) with an electrolyte solution containing 0.25 M Li_2S_6 (Figure 5, red curves). The results in Figure 5b show the thiophosphate-functionalized MOF gains a large current response with features corresponding to sulfur reduction and oxidation when the Li_2S_6 is added, whereas the parent MOF shows only a small current enhancement in Figure 5a. The symmetric cell prepared with thiophosphate additive also exhibits a smaller charge transfer resistance than the parent MOF as inferred from impedance measurements (Table S4).

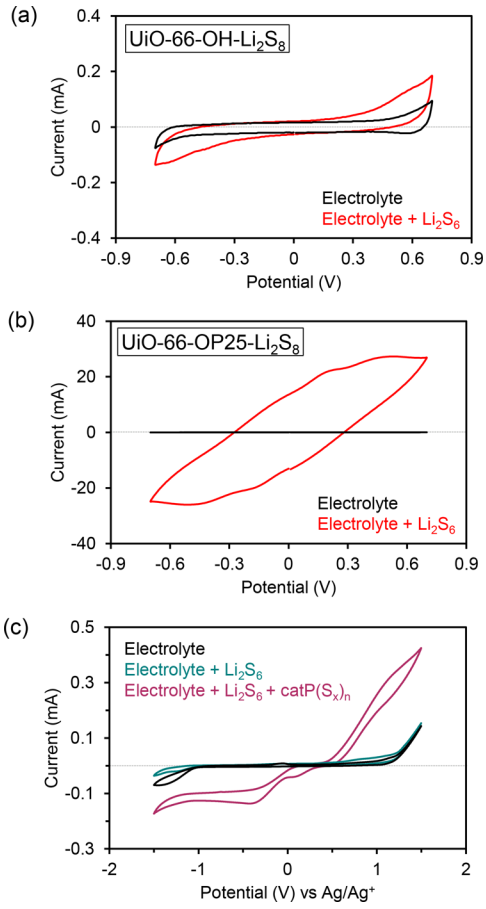

Figure 5. Cyclic voltammetry experiments conducted on symmetric cells composed of (a) UiO-66-OH-Li_2S_8 and (b) UiO-66-OP25-Li_2S_8 electrodes. The black and red curves in each graph correspond to the cell before and after addition of Li_2S_6, respectively. (c) Cyclic voltammetry experiment in a 3-electrode cell (working, counter electrodes = glassy carbon, reference electrode = Ag/Ag^+) under inert conditions in 1:1 DOL:DME in 100 mM LiTFSI and 20% (w/v) $LiNO_3$. The black curve corresponds to bare electrolyte, the teal curve to the addition of Li_2S_6 in solution, and the purple curve is the current response upon addition of $catP(S_n)_x$, confirming the phosphorus moiety facilitates polysulfide redox.

From these results, we assert that chemically tethering polysulfides to the MOF via the BDC-OP linker enhances their electrochemical accessibility, resulting in the large current enhancement and lower charge transfer resistance.

The effect of the P−S bond on polysulfide redox behavior was also explored by comparing to the molecular model of the $catP(S_n)_x$. A three-electrode system,under inert condition in 1:1 DOL:DME in 100 mM LiTFSI and 20% (w/v) $LiNO_3$, was referenced to Ag/Ag^+ with two glassy carbon electrodes serving as the working and counter electrodes. Cyclic voltammograms were obtained to determine the baseline of the electrolyte and Li_2S_6 species in these conditions (Figure 5c). Inboth cases, low currents are observed at the scanned potentials. However, upon addition of $catP(S_n)_x$, there is a significant current enhancement of both the reduction and oxidation peaks of the Li_2S_x (Figure 5c). The current enhancement is larger than the intrinsic signal from $catP(S_n)_x$ (Figure S12) without added Li_2S_6, further supporting that the phosphorus species facilitate Li−S redox.

https://doi.org/10.1021/acsaem.2c02925
ACS Appl. Energy Mater. XXXX, XXX, XXX−XXX

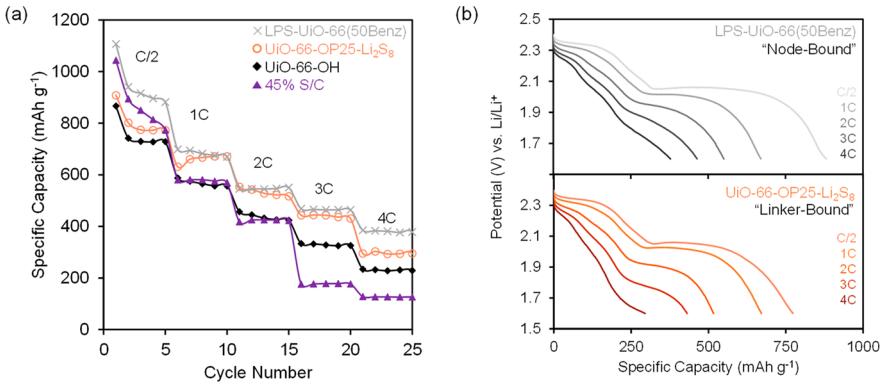

Figure 6. Rate capability results from C/2 to 4C are shown in (a). The fifth cycle's galvanostatic discharge curve at each C-rate is shown collectively in (b) for the node-functionalized LPS-UiO-66(50Benz) from our previous publication[3] and the linker-functionalized UiO-66-OP25-Li_2S_8 (bottom). At high C-rates, a third feature is seen in the discharge curves around 2.1 V vs Li/Li^+ for both cells containing thiophosphate-functionalized MOFs.

Further electrochemical analyses conducted on cycled coin cells reveal factors underpinning sulfur utilization and cyclability. Additional CV experiments on Li−S coin cells containing UiO-66-OPx additives (Figure S13) display characteristic features corresponding to sulfur redox behavior but reveal minor shifts in the Li−S redox potentials (~30 mV) compared to UiO-66-OH. Cell polarization (ΔV), quantified by extracting the potential difference from normalized galvanostatic charge/discharge curves, is provided for at 50% state of charge for cells in their 100th cycle in Table S5. Cells containing UiO-66-OPx exhibit slightly higher polarization values than the unfunctionalized or UiO-66-OPx-Li_2S_n cells, consistent with redox potential differences observed in CV experiments. Similar to the symmetric cell experiment, electrochemical impedance measurements (Table S5) reveal charge transfer resistance is lower in UiO-66-OPx-Li_2S_n compared to UiO-66-OH and UiO-66-OPx and is likely a contributing factor to increased sulfur utilization. High charge transfer resistance in UiO-66-OPx may arise from side products produced in P−Cl substitution reactions, such as adverse interaction with electrolyte or sulfur species.

In our previous study, coin cells containing the UiO-66 with the node-bound thiophosphate moiety exhibited high capacity delivery at fast charge/discharge rates (C-rates).[3] We observe similar capacity delivery for the linker-functionalized frameworks as shown in Figure 6a. Interestingly, the galvanostatic discharge curves exhibit three plateaus when cycled at C-rates above 1C (Figure 6b) for both node- and linker-functionalized MOF samples. We believe this additional feature is a partitioning of the upper plateau, a phenomenon we and others have seen in other "extreme" conditions such as low temperature or low electrolyte/sulfur ratios where mass transport becomes limiting.[5,25−27] Additional results and discharge curves are provided in Figures S14 and S15, where all cells containing phosphorus-functionalized MOFs, regardless of synthetic method or MOF identity, exhibit this behavior. Because we observe the three-plateau behavior in both thiophosphate-functionalized systems and not in any of the parent MOF cells, we attribute this effect to altered Li−S chemistry imparted by the phosphorus moiety. We are currently expanding our thiophosphate incorporation strategies and to other material platforms to investigate the electrochemical nature of this phenomenon.

CONCLUSIONS

In this work, we present a novel approach to install P−Cl and P−S moieties onto the MOF scaffold using the organic linker as an anchoring support. Spectroscopic evidence indicates that the phosphorus species is tethered via an aromatic −OH group, forming a strong P−O bond. The phosphorus-functionalized MOFs demonstrate an ability to sequester polysulfides from solution, taking up sulfur molecules in both synthetic and electrochemical experiments. We simultaneously demonstrate this chemistry in both the MOF and a model molecular system, providing spectroscopic and electrochemical evidence of reactivity and facilitated redox for both systems in parallel.

The ability of the P−Cl- and P−S-functionalized materials to capture sulfur compounds is exemplified here in Li−S batteries. Cells prepared with UiO-66-OPx and UiO-66-OPx-Li_2S_n show promising capacity retention over extended cycling and suggest phosphorus is instrumental to mitigate polysulfide leaching phenomena. Several complementary electrochemical techniques suggest the thiophosphate group also enhances sulfur utilization and lowers charge transfer resistance, both key factors to improve the energy storage capabilities of the Li−S device. While demonstrated here for sulfur capture, this P−Cl group could also be used to bind other guest molecules that form strong linkages with phosphorus with potential applications in chemical separation or sensing. This study lays foundations for synthetic capabilities to install phosphorus moieties in MOF materials, gives insight into the nature of phosphorus−polysulfide interactions, and further contributes to our understanding of the effect of chemical tethering on Li−S battery performance.

ASSOCIATED CONTENT

Supporting Information

The Supporting Information is available free of charge at https://pubs.acs.org/doi/10.1021/acsaem.2c02925.

Additional synthesis methods, NMR, IR, UV−vis absorption spectra, XRD patterns, and electrochemical measurements (PDF)

https://doi.org/10.1021/acsaem.2c02925
ACS Appl. Energy Mater. XXXX, XXX, XXX−XXX

AUTHOR INFORMATION

Corresponding Author

V. Sara Thoi − *Department of Chemistry and Department of Materials Science and Engineering, Johns Hopkins University, Baltimore, Maryland 21218, United States;* orcid.org/0000-0003-0896-4077; Email: sarathoi@jhu.edu

Authors

Avery E. Baumann − *Department of Chemistry, Johns Hopkins University, Baltimore, Maryland 21218, United States;* orcid.org/0000-0001-8513-8049

Rasha I. Anayah − *Department of Chemistry, Johns Hopkins University, Baltimore, Maryland 21218, United States;* orcid.org/0000-0001-9899-5488

Complete contact information is available at: https://pubs.acs.org/10.1021/acsaem.2c02925

Author Contributions

A.E.B. and R.I.A. contributed equally to this work.

Notes

The authors declare no competing financial interest.

ACKNOWLEDGMENTS

We thank the National Science Foundation for the CAREER Award (DMR-1945114) and a Major Research Instrumentation grant (MRI-2018176), which enabled the acquisition of a solid-state 500 MHz nuclear magnetic resonance spectrometer. We thank Drs. Jonathan Catazaro (Johns Hopkins University), David Kaplan (Argonne National Laboratory), and Fulya Dogan Key (Argonne National Laboratory) for assistance in solid-state NMR experiments. A.E.B. is grateful to receive Harry and Cleio Greer Fellowships from the Department of Chemistry and the ARCS Foundation for the Metropolitan Washington Chapter Scholar Award.

DEDICATION

R.I.A. likes to dedicate her contribution to this paper to her grandfather, who passed away in the duration of this project. In loving memory of your legacy, Sedo.

REFERENCES

(1) Nagata, H.; Chikusa, Y. A Lithium Sulfur Battery with High Power Density. *J. Power Sources* **2014**, *264*, 206−210.

(2) Lin, Z.; Liu, Z.; Fu, W.; Dudney, N. J.; Liang, C. Lithium Polysulfidophosphates: A Family of Lithium-Conducting Sulfur-Rich Compounds for Lithium-Sulfur Batteries. *Angew. Chem., Int. Ed. Engl.* **2013**, *52* (29), 7460−7463.

(3) Baumann, A. E.; Han, X.; Butala, M. M.; Thoi, V. S. Lithium Thiophosphate Functionalized Zirconium MOFs for Li−S Batteries with Enhanced Rate Capabilities. *J. Am. Chem. Soc.* **2019**, *141* (44), 17891−17899.

(4) Li, M.; Bai, Z.; Li, Y.; Ma, L.; Dai, A.; Wang, X.; Luo, D.; Wu, T.; Liu, P.; Yang, L.; Amine, K.; Chen, Z.; Lu, J. Electrochemically Primed Functional Redox Mediator Generator from the Decomposition of Solid State Electrolyte. *Nat. Commun.* **2019**, *10* (1), 1−9.

(5) Burns, D. A.; Baumann, A. E.; Bennett, K. J.; Díaz, J. C.; Thoi, V. S. Chemical Sulfide Tethering Improves Low-Temperature Li-S Battery Cycling. *ACS Appl. Mater. Interfaces* **2021**, *13* (43), 50862−50868.

(6) Baumann, A. E.; Downing, J. R.; Burns, D. A.; Hersam, M. C.; Thoi, V. S. Graphene-Metal-Organic Framework Composite Sulfur Electrodes for Li-S Batteries with High Volumetric Capacity. *ACS Appl. Mater. Interfaces* **2020**, *12* (33), 37173−37181.

(7) Zhao, Y.; Li, G.; Gao, Y.; Wang, D.; Huang, Q.; Wang, D. Stable Li Metal Anode by a Hybrid Lithium Polysulfidophosphate/Polymer Cross-Linking Film. *ACS Energy Lett.* **2019**, *4* (6), 1271−1278.

(8) Tanibata, N.; Tsukasaki, H.; Deguchi, M.; Mori, S.; Hayashi, A.; Tatsumisago, M. A Novel Discharge-Charge Mechanism of a S-P2S5composite Electrode without Electrolytes in All-Solid-State Li/S Batteries. *J. Mater. Chem. A* **2017**, *5* (22), 11224−11228.

(9) Liang, X.; Hart, C.; Pang, Q.; Garsuch, A.; Weiss, T.; Nazar, L. F. A Highly Efficient Polysulfide Mediator for Lithium−Sulfur Batteries. *Nat. Commun.* **2015**, *6*, 5682.

(10) Lin, Z.; Liu, Z.; Fu, W.; Dudney, N. J.; Liang, C. Phosphorous Pentasulfide as a Novel Additive for High-Performance Lithium-Sulfur Batteries. *Adv. Funct. Mater.* **2013**, *23* (8), 1064−1069.

(11) Cavka, J. H.; Jakobsen, S.; Olsbye, U.; Guillou, N.; Lamberti, C.; Bordiga, S.; Lillerud, K. P. A New Zirconium Inorganic Building Brick Forming Metal Organic Frameworks with Exceptional Stability - Journal of the American Chemical Society (ACS Publications). *J. Am. Chem. Soc.* **2008**, *130* (42), 13850−13851.

(12) Shearer, G. C.; Chavan, S.; Bordiga, S.; Svelle, S.; Olsbye, U.; Lillerud, K. P. Defect Engineering: Tuning the Porosity and Composition of the Metal-Organic Framework UiO-66 via Modulated Synthesis. *Chem. Mater.* **2016**, *28* (11), 3749−3761.

(13) Shearer, G. C.; Vitillo, J. G.; Bordiga, S.; Svelle, S.; Olsbye, U.; Lillerud, K. P. Functionalizing the Defects: Post Synthetic Ligand Exchange in Metal Organic Framework UiO-66. *Chem. Mater.* **2016**, *28* (20), 7190−7193.

(14) Taddei, M.; Costantino, F.; Marmottini, F.; Comotti, A.; Sozzani, P.; Vivani, R. The First Route to Highly Stable Crystalline Microporous Zirconium Phosphonate Metal-Organic Frameworks. *Chem. Commun.* **2014**, *50* (94), 14831−14834.

(15) Yabushita, M.; Li, P.; Islamoglu, T.; Kobayashi, H.; Fukuoka, A.; Farha, O. K.; Katz, A. Selective Metal-Organic Framework Catalysis of Glucose to 5-Hydroxymethylfurfural Using Phosphate-Modified NU-1000. *Ind. Eng. Chem. Res.* **2017**, *56* (25), 7141−7148.

(16) Trickett, C. A.; Osborn Popp, T. M.; Su, J.; Yan, C.; Weisberg, J.; Huq, A.; Urban, P.; Jiang, J.; Kalmutzki, M. J.; Liu, Q.; Baek, J.; Head-Gordon, M. P.; Somorjai, G. A.; Reimer, J. A.; Yaghi, O. M. Identification of the Strong Brønsted Acid Site in a Metal−Organic Framework Solid Acid Catalyst. *Nat. Chem.* **2019**, *11*, 170.

(17) Rhauderwiek, T.; Zhao, H.; Hirschle, P.; Döblinger, M.; Bueken, B.; Reinsch, H.; De Vos, D.; Wuttke, S.; Kolb, U.; Stock, N. Highly Stable and Porous Porphyrin-Based Zirconium and Hafnium Phosphonates − Electron Crystallography as an Important Tool for Structure Elucidation. *Chem. Sci.* **2018**, *9*, 5467−5478.

(18) Byrd, H.; Bharara, P. C.; Sullens, T. A.; Harden, J. D.; Gray, G. M. Preparation of Dichloro(2,4,6-Tribromophenoxy)(1,2-Diphenoxy)Phosphorane and Its Nonoxidative Chlorination Reactions with Alkyl and Aryl Phosphonates. *Inorg. Chim. Acta* **2002**, *338*, 240−244.

(19) Ramirez, F.; Bigler, A. J.; Smith, C. P. Phosphoranylations. *Tetrahedron* **1968**, *24* (14), 5041−5051.

(20) Nielsen, M. L.; Pustinger, J. V.; Strobel, J. Phosphorus-31 Nuclear Magnetic Resonance Chemical Shifts of Phosphorus Compounds. *J. Chem. Eng. Data* **1964**, *9* (2), 167−170.

(21) Lin, Z.; Liu, Z.; Dudney, N. J.; Liang, C. Lithium Superionic Sulfide Cathode for All-Solid Lithium−Sulfur Batteries. *ACS Nano* **2013**, *7* (3), 2829−2833.

(22) Yuan, Z.; Peng, H. J.; Hou, T. Z.; Huang, J. Q.; Chen, C. M.; Wang, D. W.; Cheng, X. B.; Wei, F.; Zhang, Q. Powering Lithium-Sulfur Battery Performance by Propelling Polysulfide Redox at Sulfiphilic Hosts. *Nano Lett.* **2016**, *16* (1), 519−527.

(23) Zhou, J.; Liu, X.; Zhu, L.; Zhou, J.; Guan, Y.; Chen, L.; Niu, S.; Cai, J.; Sun, D.; Zhu, Y.; Du, J.; Wang, G.; Qian, Y. Deciphering the Modulation Essence of p Bands in Co-Based Compounds on Li-S Chemistry. *Joule* **2018**, *2* (12), 2681−2693.

(24) Lin, H.; Yang, L.; Jiang, X.; Li, G.; Zhang, T.; Yao, Q.; Zheng, G. W.; Lee, J. Y. Electrocatalysis of Polysulfide Conversion by Sulfur-Deficient MoS2 Nanoflakes for Lithium-Sulfur Batteries. *Energy Environ. Sci.* **2017**, *10* (6), 1476−1486.

(25) Mikhaylik, Y. V; Akridge, J. R. Low Temperature Performance of Li -S Batteries. *J. Electrochem. Soc.* **2003**, *150*, 306−311.
(26) Gupta, A.; Bhargav, A.; Manthiram, A. Tailoring Lithium Polysulfide Coordination and Clustering Behavior through Cationic Electrostatic Competition. *Chem. Mater.* **2021**, *33* (9), 3457−3466.
(27) Jeong, S. S.; Lim, Y. T.; Choi, Y. J.; Cho, G. B.; Kim, K. W.; Ahn, H. J.; Cho, K. K. Electrochemical Properties of Lithium Sulfur Cells Using PEO Polymer Electrolytes Prepared under Three Different Mixing Conditions. *J. Power Sources* **2007**, *174* (2), 745−750.

https://doi.org/10.1021/acsaem.2c02925
ACS Appl. Energy Mater. XXXX, XXX, XXX−XXX